

Stack-of-Radial Echo Planar Imaging with Locally Low Rank Regularized Subspace Reconstruction for Fast High-Resolution Brain MRI

Zhengguo Tan¹, Erpeng Dai², and Martin Uecker^{3,4}

¹Department Artificial Intelligence in Biomedical Engineering, Friedrich-Alexander-Universität Erlangen-Nürnberg,
Erlangen, Germany

²Department of Radiology, Stanford University, Stanford, CA, 94305, United States

³Institute of Biomedical Imaging, Graz University of Technology, Graz, Austria

⁴Institute for Diagnostic and Interventional Radiology, University Medical Center Göttingen, Göttingen, Germany

July 6, 2022

Note:

Part of this article was presented at the Joint Annual Meeting ISMRM-ESMRMB & ISMRT 31st Annual Meeting, London, United Kingdom, 2022.

Correspondence to:

Dr. Zhengguo Tan
Department Artificial Intelligence in Biomedical Engineering
Friedrich-Alexander-Universität Erlangen-Nürnberg
Werner-von-Siemens-Str. 61
91052 Erlangen, Germany
Email: zhengguo.tan@fau.de

Funding information:

DFG (German Research Foundation): TA 1473/2-1, UE 189/4-1, EXC 2067/1-390729940.
NIH (National Institutes of Health): U24EB029240.

Running head:

Volumetric Radial EPI

Number of Pages: 18

Number of Figures: 5

Number of Supporting Figures: 3

Number of Supporting Videos: 1

Number of References: 31

Number of Words: 228 (abstract); ~2327 (body)

Submitted to *Magnetic Resonance in Medicine as Technical Note*

Purpose: To develop stack-of-radial echo planar imaging (EPI) with linear subspace reconstruction for volumetric, fast, and high-resolution brain magnetic resonance imaging (MRI).

Methods: We implemented the stack-of-radial EPI sequence for in vivo brain acquisition. The acquisition protocol employed flow flip angle (4 degree) excitation without fat saturation, covered the whole brain with 192 slices per volume, and utilized only 7 excitation per slice with an echo train length of 35. This allowed for fast and high-resolution brain MRI with 1 mm isotropic resolution in 1.3 min. For image reconstruction, we leveraged the linear subspace modeling method of the acquired multi-gradient-echo (MGRE) signal by constructing the truncated-SVD subspace matrix from the simulated dictionary. The subspace coefficient maps with respect to the subspace matrix were then iteratively reconstructed with locally low rank (LLR) regularization.

Results: We numerically and experimentally demonstrated that a large number of subspace coefficients were required to accurately represent the MGRE signal with off-resonance induced rapid phase modulation. In vivo brain results showed no spatial distortion artifacts in radial EPI. Excellent T_2^* contrast in the echo-combined images throughout the whole brain was achieved. Residual streaks existed likely due to the lack of proper reference scans.

Conclusion: The proposed volumetric radial EPI with advanced LLR regularized linear subspace reconstruction achieved fast and high spatial resolution brain MRI. This preliminary results showed promises for various potential brain MRI applications.

KEYWORDS

Linear Subspace, Locally low rank, Radial MRI, Echo Planar Imaging, Brain MRI.

1 INTRODUCTION

Echo planar imaging (EPI) [1] is an ultra fast and effective imaging technique, characterized by long echo train readouts per radio frequency excitation and the formation of an image from one single or a couple of excitation. Therefore, EPI has been used in various MRI applications, e.g. functional [2], diffusion [3], and arterial spin labeling imaging [4].

Although fast, the conventional EPI technique is limited to relatively low spatial resolution and suffers from spatial distortion artifacts due to off resonances. Recent progress in echo planar time resolved imaging (EPTI) using either combined gradient and spin echoes (GRASE) or multiple gradient echoes (MGRE) has achieved simultaneous multi-slice multi-parameter mapping in high spatio-temporal resolution [5]. The EPTI sequence is a multi-shot segmented multi-echo sampling method. It explores complementary sampling patterns among echoes as well as among shots and recovered multi-echo images via tilted-CAIPI reconstruction [6]. Further progress in 3D EPTI and linear subspace reconstruction has achieved 1 mm isotropic resolution and 210 slices coverage in about three minutes [7]. However, the local-patch-wise sampling of the k_y - k_z plane requires dedicated shot-to-shot B_0 variation correction algorithms.

Beside Cartesian-based EPI/EPTI techniques, radial EPI has also been proposed. One appealing feature of radial EPI is its immunity to spatial distortion artifacts [8], but early developments [9–13] achieved relatively short echo train length (i.e. smaller than 5), thereby limiting its sampling speed. Recently, Rettenmeier et al. [14] proposed 3D twisted radial EPI for functional brain MRI, where echo trains along the k_z direction were rotated (twisted) to promote incoherent k_z undersampling. Image reconstruction was then based on the CG-SENSE algorithm [15] with a pre-calibrated B_0 inhomogeneity [16] as well as coil sensitivities maps [17]. Although promising, this technique requires large blip gradients to traverse among slices.

To explore the sampling efficiency of radial sampling and to develop fast high-resolution brain imaging methods, this work proposed the k_x - k_y -plane radial EPI readouts [18, 19] combined with 3D stack-of-stars k_z sampling [20] for 1 mm isotropic brain imaging. Further, the advantage of the complementary sampling pattern in the k_x - k_y plane is exploited with the use of linear subspace modeling [21, 22] and locally low rank (LLR) regularized reconstruction [23].

2 METHODS

Radial EPI Experiments

In vivo brain MRI experiments on four young healthy adults were performed at 3 T (Skyra, Siemens Healthineers, Erlangen, Germany) with a 20-channel head coil. Written informed consents were obtained from all subjects before MRI experiments in compliance with the regulations established by the local ethics committee.

Details about our implemented sequence please refer to Supporting Information Figures S1 and S2. Similar to the original stack-of-stars sequence [20], we employed slice-selection gradients to loop over all partitions in the k_z direction, whereas radial EPI readouts were performed in the k_x - k_y plane. In addition, the standard random-RF (radio frequency) and gradient spoiling scheme was used.

Volumetric brain scans were conducted with 1 mm³ isotropic resolution. Detailed imaging parameters were: flip angle 4 degree with RF bandwidth time product of 10, in-plane field-of-view is 220 × 220 mm², base resolution 220, image matrix size 220 × 220, a total of 192 slices, bandwidth 840 Hz pixel⁻¹, 7 excitation per partition, 35 echoes per excitation with TE ranging from 1.70 to 55.7 ms (echo spacing of 1.52 ms) and TR 57.4 ms. Total scan time was 1.3 minutes. No fat saturation pulse was used before RF excitation. No k_z undersampling [24] was employed in this work.

Linear Subspace Modeling and Reconstruction

The acquired MGRE signal follows:

$$s_m = \rho \cdot e^{-\text{TE}_m/T_2^*} \cdot e^{i2\pi f_{B_0} \text{TE}_m} \quad (1)$$

where ρ is T_1 -weighted signal intensity at the echo time of 0 ms, T_2^* refers to the decay of transversal magnetization caused by a combination of spin-spin relaxation and magnetic field inhomogeneity, and f_{B_0} is the off-resonance frequency. TE_m is the echo time of the m th echo.

This work leveraged the linear subspace representation of the MGRE signal. In the MGRE signal simulation, ρ was kept as 1, with a total number of $N_\rho = 1$ atom. T_2^* linearly varied between 1 and 200 ms, with a total number of $N_{T_2^*} = 100$ values. f_{B_0} was also linearly varying with a total number of $N_{f_{B_0}} = 101$ values, but its minimal and maximal values were changed to demonstrate

the effects of f_{B_0} range on MGRE signal representation.

Therefore, the shape of the simulated dictionary is $[N_{\text{TE}}, N_\rho, N_{T_2^*}, N_{f_{B_0}}]$. We reshaped such a dictionary to two dimensional: $[N_{\text{TE}}, N_\rho \times N_{T_2^*} \times N_{f_{B_0}}]$ and denoted it as matrix D . Singular value decomposition (SVD) yields:

$$D = U\Sigma V^* \quad (2)$$

where the complex unitary matrix U has the shape $[N_{\text{TE}}, N_{\text{TE}}]$ and can be truncated to its first K ($K \leq N_{\text{TE}}$) columns, denoted as \hat{U} with the shape $[N_{\text{TE}}, K]$. Thus, the recovered echo signal is $\tilde{D} = \hat{U} \times \hat{U}^T \times D$. In this work, we iteratively increased K such that the resulting \tilde{D} satisfied $\frac{\|\tilde{D} - \tilde{D}\|}{\|D\|} \leq 10^{-5}$.

With the truncated subspace matrix \hat{U} , the linear subspace coefficient maps (α) can be reconstructed via solving

$$\underset{\alpha}{\operatorname{argmin}} \left\| y - \mathcal{F}_u S \hat{U} \alpha \right\|_2^2 + \lambda R(\alpha). \quad (3)$$

y is the measured multi-channel multi-echo k -space data. \mathcal{F}_u is the non-uniform FFT (NUFFT) [25, 26], which varies among echoes. S is one set of coil sensitivity maps, which were estimated via the nonlinear inverse reconstruction for parallel imaging using the first echo k -space data [27]. The second term in Equation (3) corresponds to regularization, in which λ is the regularization strength (set as 0.001), and $R(\alpha)$ is the locally low rank soft thresholding. Therefore, the coefficient maps α has the shape of $[N_x, N_y, K]$ with N_x and N_y the image size (i.e. base resolution).

The simulation of MGRE dictionary and the construction of the subspace matrix (\hat{U}) were performed in Python. The linear subspace reconstruction with LLR regularization were solved with The alternating direction method of multipliers (ADMM) [28] in Berkeley Advanced Reconstruction Toolbox (BART) [29]. Afterwards, the echo images can be obtained via matrix multiplication $\rho = \hat{U} \alpha$, and then the echo-combined image can be computed via the root sum square (RSS) of all echo images. All reconstructions were done on Intel Xeon Gold 6132 CPU, and the reconstruction was executed in a slice-by-slice manner, i.e. sequentially. This is possible with a slice FFT along the k_z direction of the acquired 3D k -space data [30]. For comparison, adjoint NUFFT with density compensation reconstruction of every echo was also performed with subsequent RSS operation on the coil and the echo dimensions.

3 RESULTS

Linear Subspace Modeling

Figure 1 depicts the representative results of linear subspace modeling on MGRE signal in Equation (1). Figure 1 (A) shows that when increasing the range of B_0 off-resonance frequencies in the dictionary but keeping the number of atoms consistent as 101, larger K (i.e. more subspace coefficients) is required such that the relative error between the recovered signal and the dictionary is small enough. Figure 1 (B) demonstrates that the subspace of the dictionary with maximal $|B_0|$ as 50 Hz cannot represent the simulated signal with 100 Hz off-resonance frequency. On the other hand, when increasing the maximal $|B_0|$ in the dictionary gradually toward 100 Hz, the subspace recovered signal gets closer toward the simulated signal.

Moreover, another feature of subspace modeling is the capability of representing multi compartment signal. As shown in Figure 1 (C), a summation of three species with different proton density, T_2^* , and off-resonance frequencies is simulated. The signal recovered by linear subspace modeling (with a maximal $|B_0|$ as 100 Hz in the dictionary and 31 subspace coefficients) matches well with the simulated signal.

Linear Subspace Reconstruction

Figure 2 displays three representative subspace coefficient maps from the LLR regularized linear subspace reconstruction. Since no fat saturation pulse was used in the radial EPI acquisition, the later coefficient maps (e.g. the 27th) contained mainly the tissue with large off-resonance frequencies. Plus, we also observe that the phase modulation induced by large off-resonance frequencies resulted in residual streaking artifacts in the 11th coefficient map, appearing in the frontal brain region.

Figure 3 shows the echo-combined images from three different slices in the transversal, sagittal, and coronal orientation, respectively. Firstly, our experimental results show no spatial distortion artifacts in radial EPI acquisition. Secondly, the major artifacts in radial EPI appear as radial streaks and signal void, as shown in the first slice of the transversal and the coronal views. Thirdly, the volumetric acquisition, with the use of low flip angle and long echo-train readout stack-of-radial EPI, leads to excellent T_2^* image contrast. We also appreciate the clear visibility of cerebral venous, as shown in the second slice of the sagittal view.

Please refer to Supporting Information Video S1 for the visualization of all 192 echo-combined

images with 1 mm^3 isotropic spatial resolution and a total acquisition time of only 1.3 min in three orthogonal orientations, i.e. transversal, sagittal, and coronal views. To appreciate the advantage of the LLR regularized linear subspace reconstruction, please refer to Supporting Information Figure S3 for the adjoint NUFFT reconstruction results.

Figure 4 compares the linear subspace reconstruction results from $K = 5$ and $K = 31$ in the truncated matrix \hat{U} , respectively. The $|B_0|$ range was kept consistent as 100 Hz and a total of 101 B_0 atoms in the dictionary. This experiment demonstrates that a small K cannot fully represent the signal, and thus results in not-converged image reconstruction.

On the other hand, in line with the simulation results in Figure 1, this experimentally confirms that larger K was necessary in the case of wide-range phase modulation in the dictionary of MGRE signal. The reconstruction time per slice for $K = 5$ and $K = 31$ was about 24 and 140 s, respectively. The increase of reconstruction time for larger K is expected, because larger K basically means more unknowns in the reconstructed α maps.

Noteworthy, the reconstructed image with $K = 31$ in the first column of Figure 4 is free of spatial distortion artifacts. Such an imaging slice is prone to spatial distortion and signal void in the conventional EPI technique, because of its spatial proximity to ear and nose canals filled with air. Signal void is alleviated in this case via the echo combination operation, which performs RSS of all echoes and thus avoids signal dropouts due to phase modulation.

Figure 5 shows the magnitude and phase images of the 1st, 10th, and 20th echoes, respectively. The LLR regularized linear subspace reconstruction was performed with the same dictionary as in Figure 4 and $K = 31$. Beside T_2^* signal decay, we also observe rapid phase change due to B_0 off-resonance phase modulation. Residual streaking artifacts are visible, especially in the region surrounding the skull.

4 DISCUSSION

The stack-of-radial EPI sequence presents an efficient radial sampling for fast high-resolution MRI and has the potential for other imaging modalities, e.g. functional and diffusion MRI. This work focused on its use for fast and high resolution T_2^* -weighted brain MRI. Key features of the stack-of-radial EPI trajectory are segmented radial EPI readouts in the k_x - k_y plane with seven shots and stack-of-stars [20] excitation for isotropic spatial resolution. This sequence shows potential applicability to other imaging modalities, e.g. diffusion tensor imaging and quantitative susceptibility

mapping.

Another feature of this work is the use of linear subspace modeling and LLR regularized iterative reconstruction. Adequate number of subspace coefficients presents accuracy approximation of the MGRE signal. LLR regularization is demonstrated well suited for multi-contrast images. However, the work required large number of subspace coefficients. The number of subspace coefficients can be reduced via incorporating the phase modulation term ($\Phi = e^{i2\pi f_{B_0}^T E_m}$) into the forward model in Equation (3), i.e. $F(\alpha) = \mathcal{F}_u S \Phi \hat{U} \alpha$ [31]. Here, the field inhomogeneity map (f_{B_0}) has the shape $[N_x, N_y]$ is pre-calibrated using reference scans. This approach is advantageous to reduce the number of subspace coefficients, the model complexity, and the image reconstruction time. Therefore, it would be beneficial to employ reference scans for the stack-of-radial EPI acquisition as well.

Compared with the adjoint NUFFT reconstruction in Supporting Information Figure S3, streaking artifacts in echo-combined images have been largely reduced with the LLR regularized linear subspace reconstruction. However, residual streaks are still visible in the subspace coefficient maps (Figure 2) and the individual echo images (Figure 5). These artifacts might be mitigated via the incorporation of fat saturation pulse as well as proper reference scans for the coil sensitivity and B_0 maps.

The achieved acceleration per echo in this work is $0.5\pi N_{\text{br}} / N_{\text{shot}} = 0.5\pi \times 220 / 7 \approx 49$. Here, N_{br} and N_{shot} is the base resolution and the number of shots per frame, respectively. Such high acceleration factor is achievable with the use of blip gradients. blip gradients allow for the sampling of different echoes per shot (see Supporting Information Figure S1 and S2), thereby forming a complementary sampling pattern among echoes.

In line with the standard stack-of-stars sequence [20], this radial EPI sequence utilizes aligned sampling pattern along the k_z direction. In other words, every TR block is repeated for all k_z partitions until the next TR with different segment of radial spokes (see Supporting Information Figure S1). Therefore, one potential direction would be to explore complementary k_z sampling patterns to further acceleration 3D acquisition.

Another limitation in this work is the relatively large echo spacing (1.52 ms). For EPI-type acquisition, it would be beneficial to reduce the echo spacing to about 1 ms [31]. shorter echo spacing can accelerate echo acquisition and reduce susceptibility artifacts. Therefore, it would be logic to identify contributing factors in the sequence which constraint the bandwidth as well as the echo spacing.

5 CONCLUSION

We propose a fast and high-resolution brain MRI method that combined stack-of-radial radial EPI for volumetric acquisition with advanced LLR regularized linear subspace reconstruction. Our developed radial EPI sequence exploits complementary sampling patterns among echoes in the k_x - k_y plain, whereas for 3D acquisition radial spoke segments of every shot are aligned along the k_z direction. LLR regularization presents an effective method for multi-contrast image reconstruction.

OPEN RESEARCH

In the spirit of reproducible and open research, the proposed method is made openly available as part of BART ¹. Scripts and data to reproduce the experiments will be made public upon the publication of the manuscript.

Acknowledgment

The authors thank Prof. Dr. Florian Knoll for proofreading the paper.

¹<https://github.com/mrirecon/bart/>

REFERENCES

- [1] Mansfield P. Multi planar image formation using NMR spin echoes. *J Phys C* 1977;10:L55–L58.
- [2] Ogawa S, Lee TM, Kay AR, Tank DW. Brain magnetic resonance imaging with contrast dependent on blood oxygenation. *Proc Natl Acad Sci* 1990;87:9868–9872.
- [3] Le Bihan D, Breton E, Lallemand D, Grenier P, Cabanis E, Laval-Jeantet M. MR imaging of intravoxel incoherent motions: application to diffusion and perfusion in neurologic disorders. *Radiology* 1986;161:401–407.
- [4] Feinberg DA, Beckett A, Chen L. Arterial spin labeling with simultaneous multi-slice echo planar imaging. *Magn Reson Med* 2013;70:1500–1506.
- [5] Wang F, Dong Z, Reese TG, Bilgic B, Manhard MK, Chen J, et al. Echo planar time-resolved imaging. *Magn Reson Med* 2019;81:3599–3615.
- [6] Dong Z, Wang F, Reese TG, Manhard MK, Bilgic B, Wald LL, et al. Tilted-CAIPI for highly accelerated distortion-free EPI with point spread function (PSF) encoding. *Magn Reson Med* 2019;81:377–392.
- [7] Dong Z, Wang F, Chan KS, Reese TG, Bilgic B, Marques JP, et al. Variable flip angle echo planar time-resolved imaging (vFA-EPTI) for fast high-resolution gradient echo myelin water imaging. *NeuroImage* 2021;232:1–12.
- [8] Silva AC, Barbier EL, Lowe IJ, Koretsky AP. Radial Echo-Planar Imaging. *J Magn Reson* 1998;135:242–247.
- [9] Seifert MHJ, Jakob PM, Jellus V, Haase A, Hillenbrand C. High-resolution diffusion imaging using a radial turbo-spin-echo sequence: Implementation, eddy current compensation, and self-navigation. *J Magn Reson* 2000;144:243–254.
- [10] Theilmann RJ, Gmitro AF, Altbach MI, Trouard TP. View-ordering in radial fast spin-echo imaging. *Magn Reson Med* 2004;51:768–774.
- [11] Jung Y, Samsonov AA, Block WF, Lazar M, Lu A, Liu J, et al. 3D diffusion tensor MRI with isotropic resolution using a steady-state radial acquisition. *J Magn Reson Imaging* 2009;29:1175–1184.

- [12] Lee GR, Griswold MA, Tkach JA. Rapid 3D radial multi-echo functional magnetic resonance imaging. *NeuroImage* 2010;52:1428–1443.
- [13] Bhat H, Yang Q, Zuehlsdorff S, Li K, Li D. Contrast-enhanced whole-heart coronary magnetic resonance angiography at 3 T with radial EPI. *Magn Reson Med* 2011;66:82–91.
- [14] Rettenmeier CA, Maziero D, Stenger VA. Three dimensional radial echo planar imaging for functional MRI. *Magn Reson Med* 2021;87:193–206.
- [15] Pruessmann KP, Weiger M, Börnert P, Boesiger P. Advances in sensitivity encoding with arbitrary k-space trajectories. *Magn Reson Med* 2001;46:638–651.
- [16] Funai AK, Fessler JA, Yeo DTB, Olafsson VT, Noll DC. Regularized field map estimation in MRI. *IEEE Trans Med Imaging* 2008;27:1484–1494.
- [17] Walsh DO, Gmitro AF, Marcellin MW. Adaptive reconstruction of phased array MR imagery. *Magn Reson Med* 2000;43:682–690.
- [18] Tan Z. Advances in real-time phase-contrast flow MRI and multi-echo radial FLASH. PhD thesis, University of Göttingen; 2016.
- [19] Tan Z, Voit D, Kollmeier JM, Uecker M, Frahm J. Dynamic water/fat separation and B_0 inhomogeneity mapping – Joint estimation using undersampled triple-echo multi-spoke radial FLASH. *Magn Reson Med* 2019;82:1000–1011.
- [20] Block KT, Chandarana H, Milla S, Bruno M, Mulholland T, Fatterpekar G, et al. Towards routine clinical use of radial stack-of-stars 3D gradient-echo sequences for reducing motion sensitivity. *J Korean Soc Magn Reson Med* 2014;18:87–106.
- [21] Huang C, Graff CG, Clarkson EW, Bilgin A, Altbach MI. T_2 mapping from highly undersampled data by reconstruction of principal component coefficient maps using compressed sensing. *Magn Reson Med* 2012;67:1355–1366.
- [22] Tamir JI, Uecker M, Chen W, Lai P, Alley MT, Vasanawala SS, et al. T_2 shuffling: Sharp, multicontrast, volumetric fast spin-echo imaging. *Magn Reson Med* 2017;77:180–195.
- [23] Zhang T, Pauly JM, Levesque IR. Accelerated parameter mapping with a locally low rank constraint. *Magn Reson Med* 2015;73:655–661.

- [24] Feng L, Zhao T, Chandarana H, Sodickson DK, Otazo R. Motion-resolved golden-angle radial sparse MRI using variable-density stack-of-stars sampling. In: Proceedings of the 24th Annual Meeting of ISMRM, Singapore, Singapore; 2016. p. 1091.
- [25] Fessler JA, Sutton BP. Nonuniform fast Fourier transforms using min-max interpolation. *IEEE Trans Signal Process* 2003;51:560–574.
- [26] Beatty PJ, Nishimura DG, Pauly JM. Rapid gridding reconstruction with a minimal oversampling ratio. *IEEE Trans Med Imaging* 2005;24:799–808.
- [27] Uecker M, Hohage T, Block KT, Frahm J. Image reconstruction by regularized nonlinear inversion – Joint estimation of coil sensitivities and image content. *Magn Reson Med* 2008;60:674–682.
- [28] Boyd S, Parikh N, Chu E, Peleato B, Eckstein J. Distributed optimization and statistical learning via the alternating direction method of multipliers. *Foundations and Trends in Machine Learning* 2010;3:1–122.
- [29] Uecker M, Ong F, Tamir JI, Bahri D, Virtue P, Cheng JY, et al. Berkeley Advanced Reconstruction Toolbox. In: Proceedings of the 23th Annual Meeting of ISMRM, Toronto, CAN; 2015. p. 2486.
- [30] Feng L, Grimm R, Block KT, Chandarana H, Kim S, Xu J, et al. Golden-angle radial sparse parallel MRI: Combination of compressed sensing, parallel imaging, and golden-angle radial sampling for fast and flexible dynamic volumetric MRI. *Magn Reson Med* 2014;72:707–717.
- [31] Dong Z, Wang F, Reese TG, Bilgic B, Setsompop K. Echo planar time-resolved imaging with subspace reconstruction and optimized spatiotemporal encoding. *Magn Reson Med* 2020;84:2442–2455.

LEGENDS TO THE FIGURES

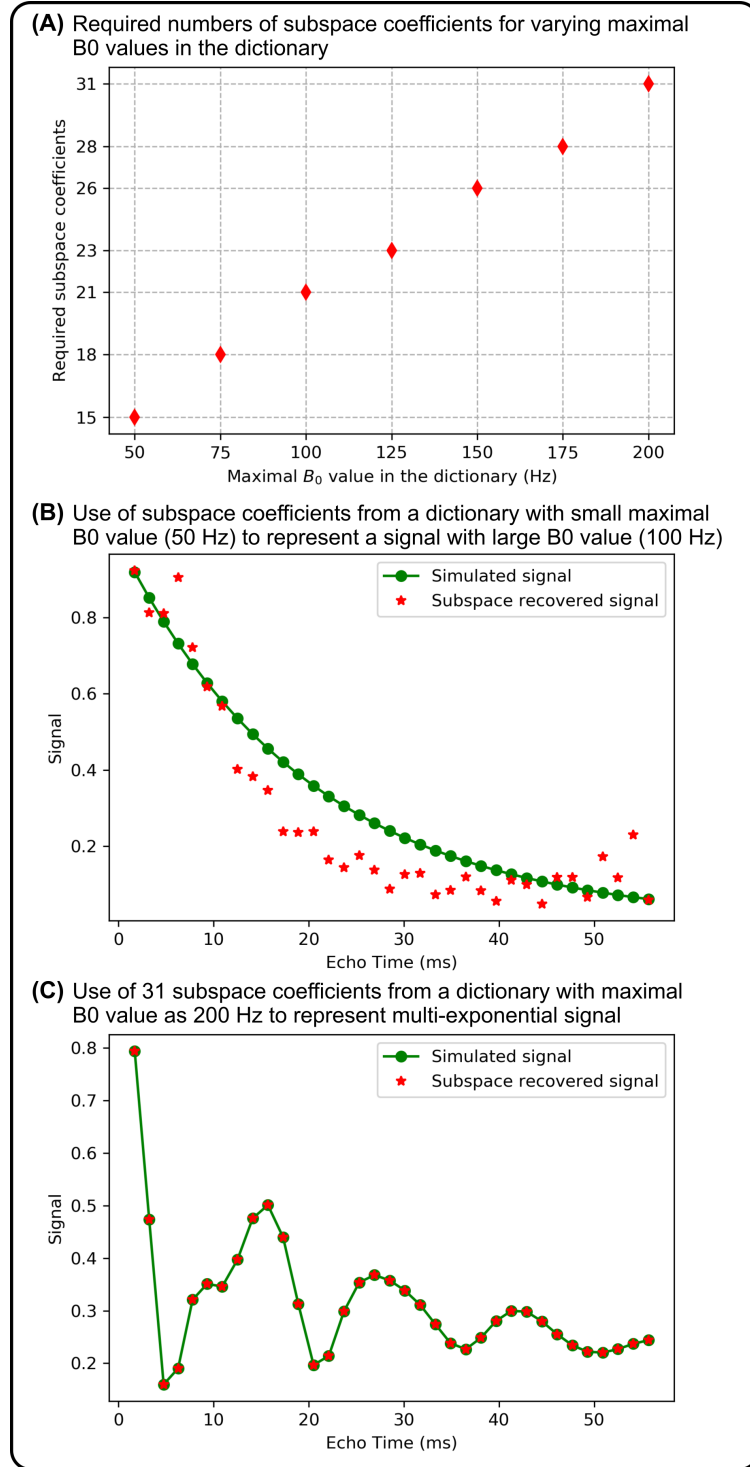


Figure 1 Linear subspace simulations of multi-gradient-echo (MGRE) signals. **(A)** When increasing the maximal B_0 values (minimum is minus maximum of B_0) in MGRE signal dictionary simulation, the required number of subspace coefficients increases. **(B)** The use of only 15 subspace coefficients from a dictionary with a small maximal B_0 value (50 Hz) can not represent a signal with large B_0 value (100 Hz). **(C)** Subspace modeling can represent multi-exponential signal. The simulated signal contains proton density with values 0.3, 0.3 and 0.4, T_2^* with values 20, 10 and 100 ms, and off-resonance frequencies with values 50, 100 and -20 Hz, respectively.

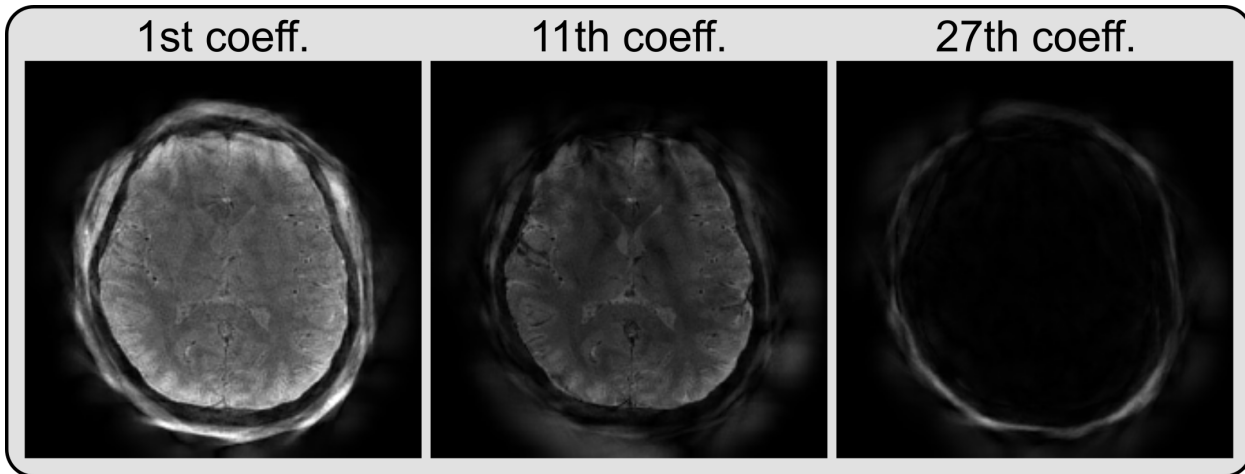


Figure 2 Representative subspace coefficient maps from the linear subspace reconstruction. In the 27th coefficient, only the fat layer with large off-resonance frequencies is visible.

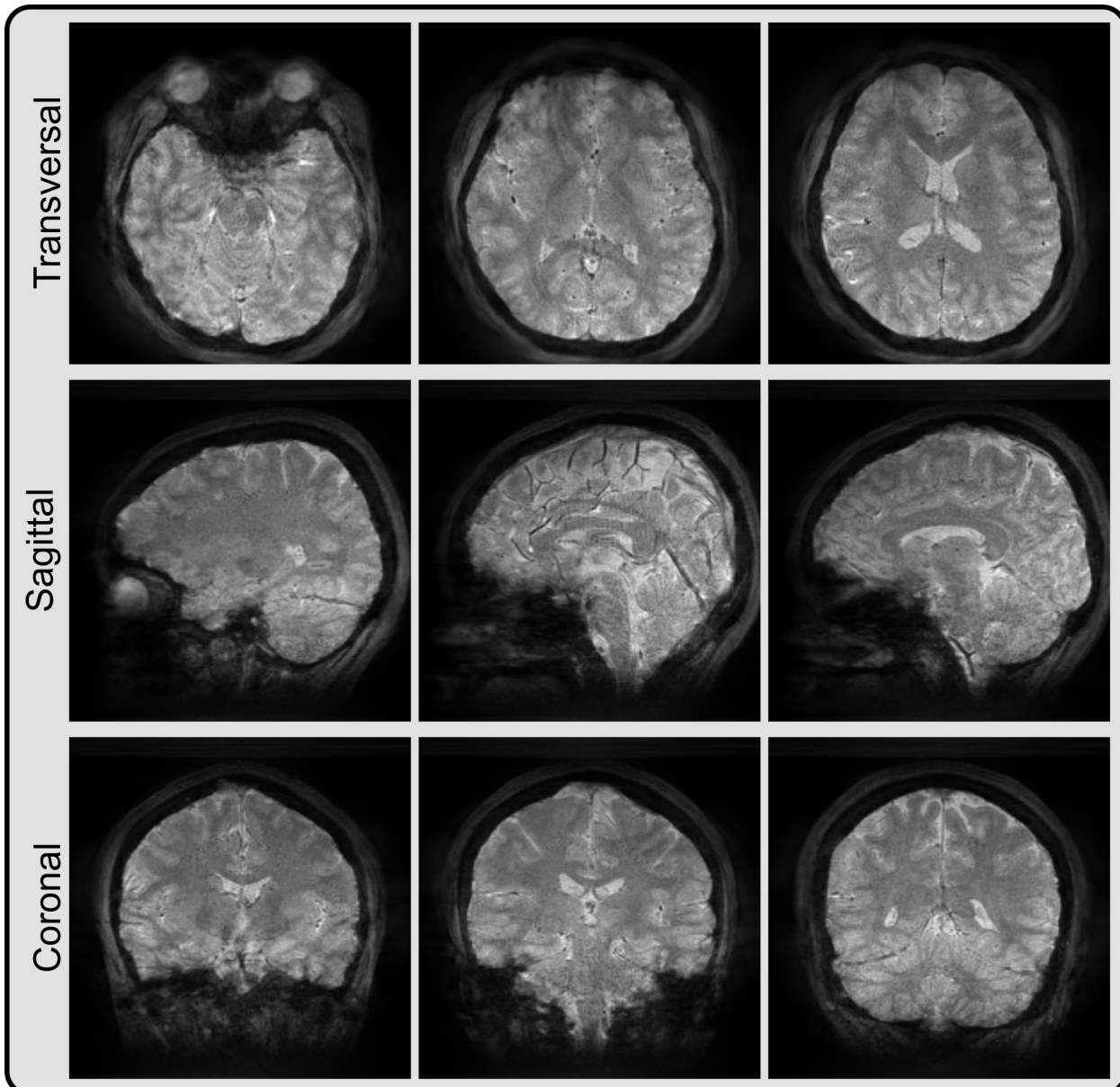


Figure 3 Representative slices of the echo-combined images: (top) transversal, (middle) sagittal, and (bottom) coronal views. Three slices from every view orientation are selected for display.

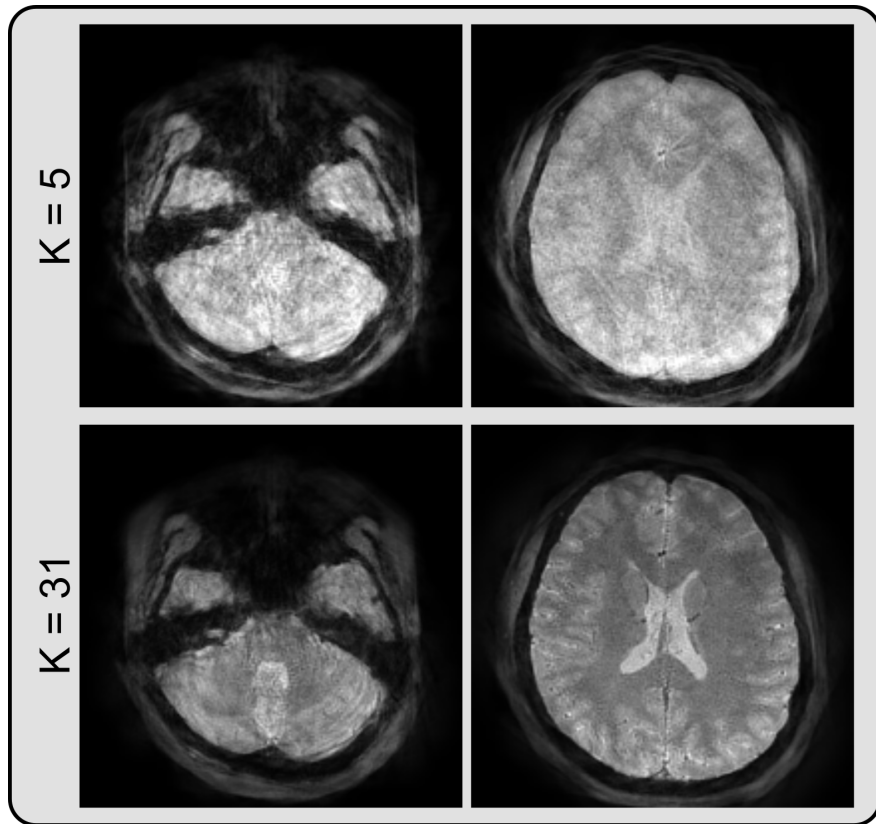


Figure 4 Echo-combined images from the linear subspace reconstruction using (top) 5 and (bottom) 31 coefficients in the truncated matrix \hat{U} , respectively. The B_0 values in the dictionary is kept consistent, i.e. linearly varying from -100 to 100 Hz with 101 atoms.

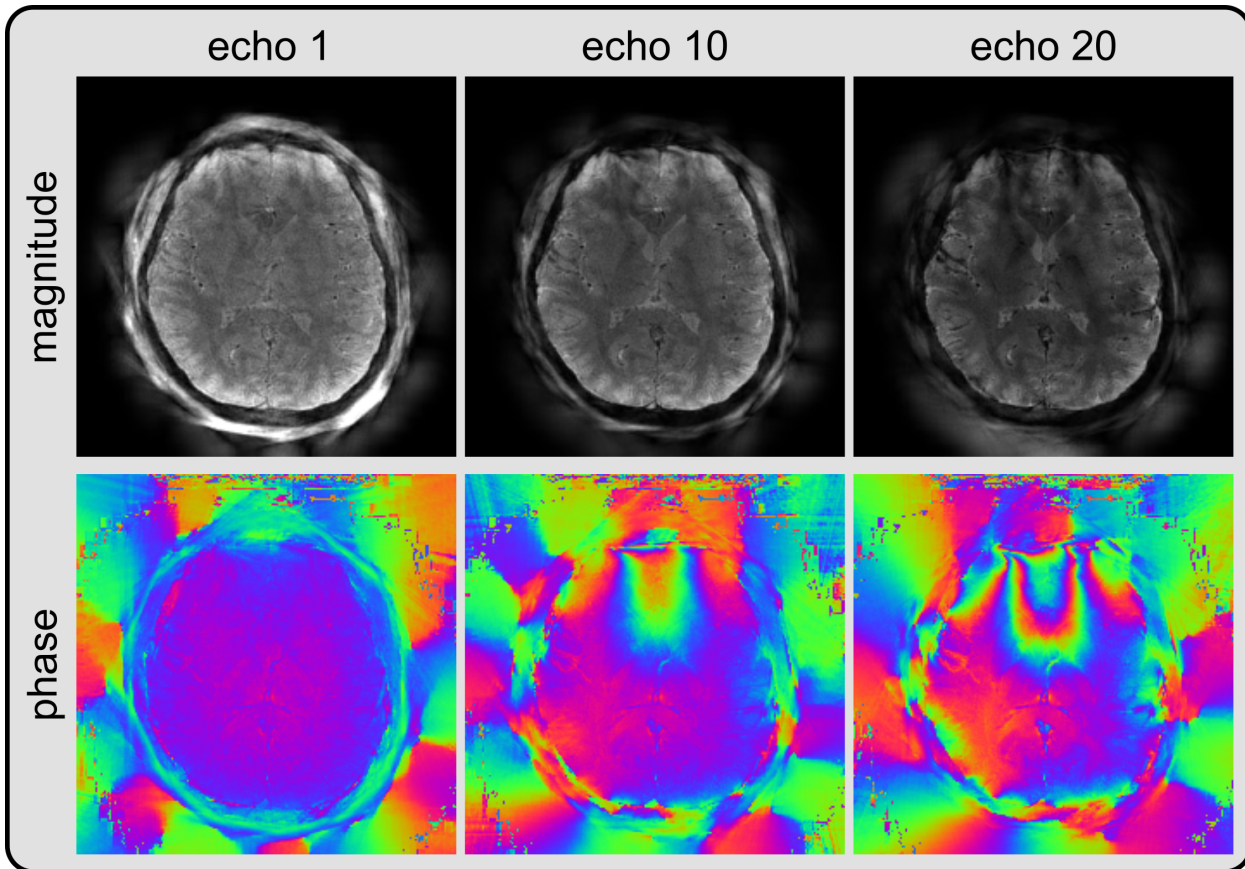


Figure 5 The magnitude and phase images of the 1st, 10th, and 20th echoes via linear subspace reconstruction with the same dictionary as in Figure 4 and $K = 31$.

SUPPORTING INFORMATION

Additional Supporting Information may be found online in the Supporting Information section.

Figure S1. (Top) Screenshot of the segmented radial EPI sequence implemented on Siemens pulse sequence programming platform. In this work, one complete k -space consists of seven excitation (segments). (Bottom) Zoomed-in sequence diagram of the third TR block. Note that this simulation presents the case of 2D acquisition. For 3D acquisition, every TR block is repeated for all k_z partitions until the next TR block with different segment of radial spokes.

Figure S2. Color-coded illustration of the radial EPI sequence from one excitation and its corresponding k -space trajectory. The elongated black line after the readout of the last echo represents the spoiling gradients.

Figure S3. Adjoint NUFFT with density compensation reconstruction results of the same slices and orientation views as in Figure 3.

Video S1. The echo-combined images from the total 192 slices in three orientation views.